Journal of Manufacturing Processes 97 (2023) 1–11

Contents lists available at ScienceDirect

Journal of Manufacturing Processes

journal homepage: www.elsevier.com/locate/manpro

Strength and microstructure of friction stir welded additively manufactured Scalmalloy® in as-welded and heat-treated conditions

Pietro Mirandola [a], Vincenzo Lunetto [b,*], David Novel [a], Mario Barozzi [a], Pierluigi Bellutti [c], Manuela De Maddis [b], Pasquale Russo Spena [b]

[a] MNF-Micro Nano Facility, Sensors & Devices Center, Bruno Kessler Foundation, Via Sommarive 18, 38123 Trento, Italy
[b] Department of Management and Production Engineering, Politecnico di Torino, Corso Duca degli Abruzzi 24, 10129 Torino, Italy
[c] Bruno Kessler Foundation, Via Sommarive 18, 38123 Trento, Italy

ARTICLE INFO

Keywords:
Friction stir welding
Additively manufactured Scalmalloy®
Butt joint
Mechanical strength
Microstructure
Age hardening heat treatment

ABSTRACT

This study investigates the feasibility of butt friction stir welding of LPBF additively manufactured FSW Scalmalloy® plates, assessing the microstructural and mechanical properties of the joints in as-welded and heat-treated conditions. The heat treatment consisted of age hardening to benefit from the strengthening effect of Al-Sc precipitates on the FSW joint strength. The influence of the build direction of the additive layers on joint microstructure and mechanical performances has also been determined.

The results show that the build direction of the Scalmalloy® plates affects neither the FSW process nor the microstructural and mechanical properties of the welded joints. The FSW thoroughly modifies the microstructures of the as-printed Scalmalloy®, eliminating the intrinsic porosity associated with the AM process. The heat input in the welding process causes the precipitation of Al-Sc phases so that the following aging heat treatment has a limited effect on improving joint strength. Although the Al-Sc strengthening enhances the strength and hardness of Scalmalloy®, there is a significant loss of ductility (from 16 % to 4 %), as also pointed out by the absence of plastic deformation on the surface fracture of the heat-treated tensile samples.

1. Introduction

The main limit of commercial wrought and cast aluminum alloys is that they cannot be used for high-temperature applications over the 200–300 °C range [1]. Aluminum alloys soften significantly at these temperatures, and the second-phase hardening effect disappears because of the coarsening of the strengthening precipitates. Therefore, more high-resistant metals, such as Fe-, Ti-, and Ni-based alloys, are commonly used for structural applications at high temperatures, despite some issues concerning their high density and costs [2,3].

In recent years, advanced aluminum alloys with unique chemical compositions and microstructures have been developed to overcome the above-mentioned technological drawbacks. Three types of solutions have been exploited to improve the mechanical resistance of such alloys at high temperatures, the use of: 1) Al-based strengthening particles that are more stable at high temperatures; 2) ceramic dispersoids (e.g., carbides, oxides, nitrides, and borides); 3) intermetallics (e.g., HiFI alloys). In this scenario, high-strength heat-treatable aluminum-scandium alloys were developed in the seventies in the United States and the Soviet Union, mainly for the military industry [4]. For such alloys, precipitation hardening heat treatment (solubilization + aging) promotes the formation of extremely small and uniformly dispersed Al-Sc-Zr second-phase particles (mostly $Al_3(Sc, Zr)$) within the parent metal matrix, which contributes the most to the increased mechanical strength [5,6].

In the last few years, aluminum-scandium alloys have been developed for AM purposes with the trade name Scallmalloy®. Apworks GmbH has patented the chemical composition of Scallmalloy® for the laser powder bed fusion (LPBF) technology, thus demonstrating the AM processability of this alloy [5]. Components with a density higher than 99 % have been obtained using a laser power of 200–400 W, a layer thickness of 30 μm, and a volumetric energy density (VED) of about 120 J/mm^3 [6]. Martucci et al. [7] increased VED to 175 J/mm^3 to achieve a density higher than 99 % with a laser power of 100 W and a layer thickness of 15 μm. Qbau et al. [8] investigated a combination of different laser power values (200–375 W) and a layer thickness of 40 μm to obtain a density higher than 99 % in the 55–70 J/mm^3 range. In

* Corresponding author.
E-mail address: vincenzo.lunetto@polito.it (V. Lunetto).

https://doi.org/10.1016/j.jmapro.2023.04.051
Received 13 February 2023; Received in revised form 17 April 2023; Accepted 20 April 2023
Available online 1 May 2023

several applications, AM Scallmalloy® can effectively replace more traditional AM alloys like AlSi10Mg, AlSi7Mg, and AlSi12. However, its mechanical properties depend to a great extent on the LPBF process (i.e., process parameters) and the post-heat treatment. The yield (YS) and ultimate tensile strength (UTS) of AM Scallmalloy® are usually 300–500 MPa and 350–500 MPa, respectively [6,9], with a hardness of 95–170 HV [7,10,11]. More in detail, Ma et al. [9] and Spierings et al. [12] found that the tensile strength of Scalmalloy® can be increased from 350 to over 530 MPa with age hardening at 325–350 °C for a duration between 4 and 10 h. However, the greater mechanical strengths were associated with a reduction in ductility: elongation at fracture of 2–8 % vs. at least 10 % for the as-printed samples. AM Scallmalloy® shows the typical bi-modal microstructure made of coarse columnar and fine equiaxed grains due to the LPBF technology. Ma et al. [12] found that this microstructure did not change with age hardening because Al_3(Sc, Zr) particles along the grain boundary prevented grain growth. The authors also found that age hardening over 350 °C promoted the coarsening of Al_3(Sc, Zr) and Al_6Mn particles associated with reduced strength. Zhang et al. [11] investigated the effect of the laser scan speed on the size and distribution of Al_3(Sc, Zr) precipitates. Lower scan speeds (1800 mm/s) favored the formation of coherent and spherical Al_3(Sc, Zr) precipitates with 10–40 nm size, increasing hardness and wear resistance. Higher laser scan speeds (3000 mm/s) did not induce the formation of Al_3(Sc, Zr) precipitates in the matrix.

An increasing interest in AM Scalmalloy® has been observed in several industrial fields to produce low-density and strength components at high temperatures, such as satellites, trabecular structures for fuselage dividers, heat exchangers, and parts for motorsport competitions. Such alloys must often be assembled together or with other metals through welding. Like more traditional aluminum alloys, Scalmalloy® also suffers from assembly operations whenever such operations are realized through fusion welding technologies. The melting and subsequent solidification of the molten pool completely disrupt the original microstructures and mechanical properties of the base metals, with the weldment exhibiting coarse and brittle microstructures.

Friction Stir Welding (FSW) is the most effective way of overcoming the issues of fusion welding technologies and, hence, preserving the engineered microstructures. FSW is a well-established technology for solid-state joining conventional wrought Al alloys, especially for the aeronautic and aerospace industries [13,14]. Some studies have been conducted on the FSW of bulk Al-Mg-Sc and Al-Mg-Sc-Zr sheets and plates produced by flat rolling. Zhao et al. [15] reported that the FSW joints of Al-Mg-Sc alloys could achieve higher tensile and yield strengths of 20 % and 30 %, respectively, than those obtained from equivalent GTAW joints. They found that FSW altered the hardness of the base metal less, which moved from 130 HV to 115 HV in the HAZ. On the other hand, the larger heat input involved in the GTAW process led to a significant drop in hardness, that is, to 95 HV. The greater reduction in hardness was mainly associated with the partial solubilization [15,16] and coarsening [17] of Al_3(Sc, Zr) precipitates. Sauvage et al. [16] compared the influence of nano-sized precipitates on the microstructures of FSW joints of Al-Mg-Si and Al-Mg-Sc alloys. Al_3Sc precipitates markedly pinning the grain boundaries of the weld recrystallized grains and preventing grain growth in the weld nugget. These effects were much more limited in Al-Mg-Si alloys. Malopheyev et al. [17] evaluated the mechanical properties of FSW joints of ultra-fine-grained Al-Mg-Sc-Zr sheets obtained by means of hot (UTS 440 MPa, elongation at fracture, e_f, 11.5 %) and cold (UTS 565 MPa, e_f 5.5 %) rolling. They found that the FSW joints obtained from cold rolled sheets were more sensitive to the joining process: the joint strength was reduced by more than 40 %, whereas it was only 15 % less for the joints obtained from hot rolled sheets. Instead, the different rolling procedures did not affect the ductility of the FSW joints, which only reduced by 1–2 %.

All the studies mentioned above refer to bulk components, and there are only a few works in the literature about the FSW of traditional additively manufactured Al alloys, including AlSi10Mg and AlSi12. Al-Sc alloys have yet to be investigated, and only some preliminary works are ongoing (e.g., the OASIS project funded by the European Union [18]). Scherillo et al. [19] found that FSW completely modified the typical layer-by-layer morphology of the microstructure of as-printed AlSi10Mg alloys. The stirring action of the tool led to grain recrystallization and refinement of the stir zone (SZ) and the thermo-mechanically affected zone (TMAZ), to a homogenization of the microstructure, and a reduction in the intrinsic porosity associated with an improvement of joint toughness. Du et al. [20] reported that the joining process reduced the mechanical strength of AlSi10Mg FSW welds. The as-printed metal exhibited yield and tensile strengths of 265 and 451 MPa, respectively, whereas those of the FSW joints were 146 and 240 MPa under optimal welding conditions. Specifically, the mechanical strength and ductility of the FSW joints varied according to the heat input provided during the welding process. Too low heat inputs provided less-resistant joints, with yield and tensile strengths reduced to 110 and 132 MPa. Elongation at fracture changed from 2.2 to 8.3 % (6.3 % for the as-printed material). Moeini et al. [21] investigated the effect of the build orientation on the properties of FSW joints made from AlSi10Mg coupons manufactured by an SLM 280^{HL} system. The as-printed coupons obtained with a build direction perpendicular to the tensile load showed a higher UTS and elongation at fracture of 6 % and 30 %, respectively, than those achieved for the samples with a build direction along the load. Similar differences among the coupons were observed after welding: a higher UTS and elongation at fracture of 3 % and 50 %, respectively, for the samples printed perpendicularly to the load direction. Eff et al. [22] investigated the influence of age-hardening heat treatment on the mechanical properties of FSW joints made of AlSi10Mg coupons obtained from an EOS M 290 PBF-L machine. The welds were first annealed at 530 °C for 6 h. Two different treatments were then carried out: 1) quenching in water; 2) quenching in water and artificially aging at 160 °C for 2 h. The tensile strength and the elongation at fracture reduced by 5 % and 9 % for the only quenched samples, compared with the as-printed material, but they decreased by 78 % and 83 % for the aged samples. Prashanth et al. [23] evaluated the mechanical and microstructural properties of FSW joints of AlSi12. The welded joints showed a reduction in hardness (80 HV in the SZ vs. 95 HV) and mechanical strength (yield strength reduced from 260 to 215 MPa), compared to the as-printed metal, but a notable increase in elongation at fracture (from 3 to 10 %). The different mechanical properties of the FSW joints were mainly attributed to significant growth in the sizes of the Al and Si phases. Moeini et al. [24] reported similar results for the FSW of AlSi12.

This work investigates the FSW of Scalmalloy® and the microstructural and mechanical properties of the resulting welded joints. Plates (4 mm thick) were obtained through LPBF, and then butt FSW welded. Some samples were also subjected to aging heat treatment to assess the strengthening effect on the mechanical performances of the welds. The microstructure of the FSW joints was assessed via SEM and EBSD techniques, while the mechanical properties were evaluated through standard hardness and tensile tests. The influence of the build direction on the real-time process parameters (i.e., tool spindle torque, vertical and advancing force) and the weld properties have also been investigated.

2. Materials and methods

Scalmalloy® plates (4 mm thick, 75 mm long, and 55 mm wide) were additively manufactured via the LPBF technology with a Mlab cusing R machine. According to the supplier technical datasheet, the Scalmalloy® powder had a grain size distribution over the 20–63 μm range and the chemical composition reported in Table 1. After an experimental pilot campaign, the following parameters were used during the metal printing: laser spot diameter of 50 μm, laser power of 95 W, scan speed of 400 mm/s, hatch spacing of 63 μm, and layer thickness of 15 μm. Overall, sixteen plates were printed with two different orientations: eight plates were printed with the longer size parallel to the build direction (type

Table 1
Chemical composition (wt%) of the Scalmalloy® powder, as from the supplier technical datasheet.

Mn	Si	Co	Mg	Zr	Zn	V	Sc	Fe	Ti	O	Al
0.30–0.80	0.40	0.10	4.20–5.10	0.20–0.50	0.25	0.10	0.60–0.88	0.40	0.15	0.05	Bal.

"A"), while the other eight plates were printed along the perpendicular direction (type "B"). Fig. 1 shows an example of a job realized by means of LPBF. The density measured in the two configurations is slightly different since the build direction influences this factor. "A" samples had a density of 98.0 ± 0.1 %, while the density of the "B" samples was 99.2 ± 0.1 %.

To properly join the AM coupons, a preliminary experimental campaign was conducted to determine the process parameters, including plunge deep, plunge speed, dwell time, rotation speed, and welding speed. The process parameters for the FSW campaign on the AM Scalmalloy® plates are listed in Table 2. Couples of plates with the same build orientation were butt welded along the longer sides to evaluate the effect of the layer orientation on the mechanical properties of the FSW joints. The welding tests were performed using a 100 kN FSW machine (Stirtec GmbH) with a water-cooled spindle, available at the J-Tech interdepartmental laboratory of the Politecnico di Torino, Fig. 2 a). The FSW tool had a flat shoulder and a truncated cone pin, as shown in Fig. 2 b). A flat shoulder was selected to avoid excessive tool wear of the sharp corners typical of convex and tapered shoulders. The tool was made of a tungsten-rhenium alloy (75 wt% W, 25 wt% Re) to withstand the high temperatures reached during the welding. An argon shielding gas was flown over the weld to protect it from oxidation. The gas was fed through two nozzles at the front and rear of the FSW tool. Four FSW seams were realized for each 3D build direction to obtain consistent results for the mechanical characterization of the joints.

Scalmalloy® is usually heat-treated to exploit the strengthening effect of the Al-Sc second phases. Similarly, the welded coupons were aged after FSW. The aging heat treatment was conducted in air at 325 °C for 4 h according to the works of Li et al. [25] and Jia et al. [26] on Al-Sc alloys.

Samples were extracted from the welding coupons before and after the aging heat treatment, and then subjected to mechanical tests and microstructural examination, Fig. 3. The strength of the FSW joints was assessed through tensile tests on dogbone samples, Fig. 3 a). The samples were cut from each weld using wire electrical discharge machining, adopting the geometry recommended by the DIN 50125 standard [27]. The trials were carried out on a standard testing machine with a cross-head speed of 0.63 mm/min. The cross-sections of the FSW joints were

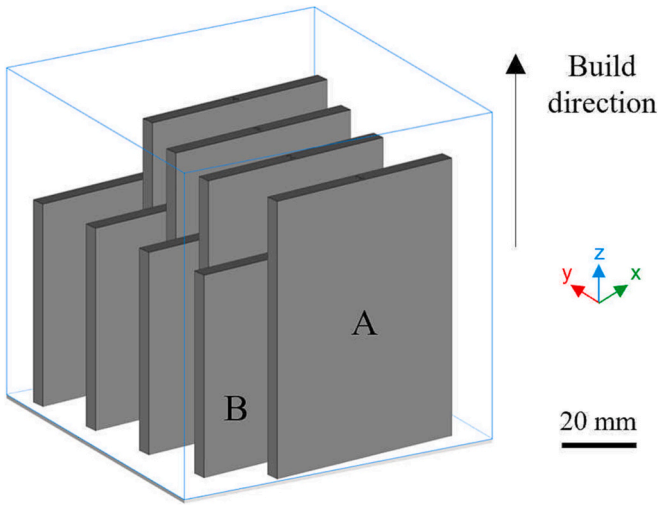

Fig. 1. The two printed orientations of the Scalmalloy® plates used in the FSW tests.

Table 2
Process parameters for the FSW campaign on the AM Scalmalloy® plates.

Tilt angle [°]	Plunge deep [mm]	Plunge speed [mm/min]	Dwell time [s]	Rotation speed [rpm]	Welding speed [mm/min]
2	3.7	3	2	1500	400

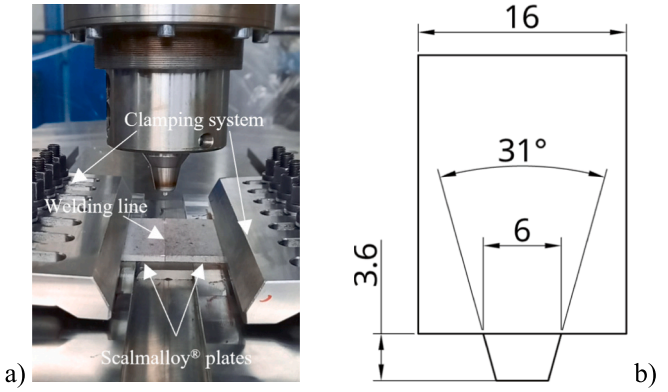

Fig. 2. a) FSW equipment and b) tool geometry used for the welding tests.

examined using optical and SEM microscopy. The metallographic samples were prepared using a standard procedure, which included grinding, polishing, and a final chemical etching with a Keller's reagent. The grain size and orientation were assessed using an EBSD analysis according to the ASTM E2627 standard [28]. The EBSD tests were conducted using a Bruker high-resolution e-FlashHR detector installed in a ThermoFisher Helios 5 PFIB CXe DualBeam. The Helios 5 system was equipped with a vertical SEM column and a Xe+ ions column tilted at 52°. The EBSD samples were prepared with a standard mechanical polishing procedure and then polished by ion sputtering. The ion sputtering was performed within the Helios 5 analytical chamber under a high vacuum with a 360 nA of Xe+ ions current at 12 keV of impact energy and 22° of incidence angle, sputtering time was calibrated to avoid damaging the sample surface [29]. After the polishing, the samples remained in a high vacuum to perform the EBSD measurements. The EBSD maps were acquired on 70° tilted samples with an electron current of 13 nA at 15 keV.

The hardness of the base metal (BM), HAZ, TMAZ, and SZ, was evaluated throughout the cross-section of the joints through Vickers microhardness measurements. The tests were conducted according to the ASTM E92 standard [30] with a 500 g load and a distance of 1 mm was kept between two successive indentations. Vickers microhardness maps of the cross-sections of the FSW joints were obtained using RStudio software.

3. Results and discussion

3.1. FSW process parameters

Fig. 4 shows the typical torque and tool forces (vertical and advancing directions) monitored during the welding of the FSW joints. The monitored parameters do not vary among the joints; therefore, the build direction of the printed coupons has not affected the joining process. The vertical force at the beginning of the plunge phase rapidly

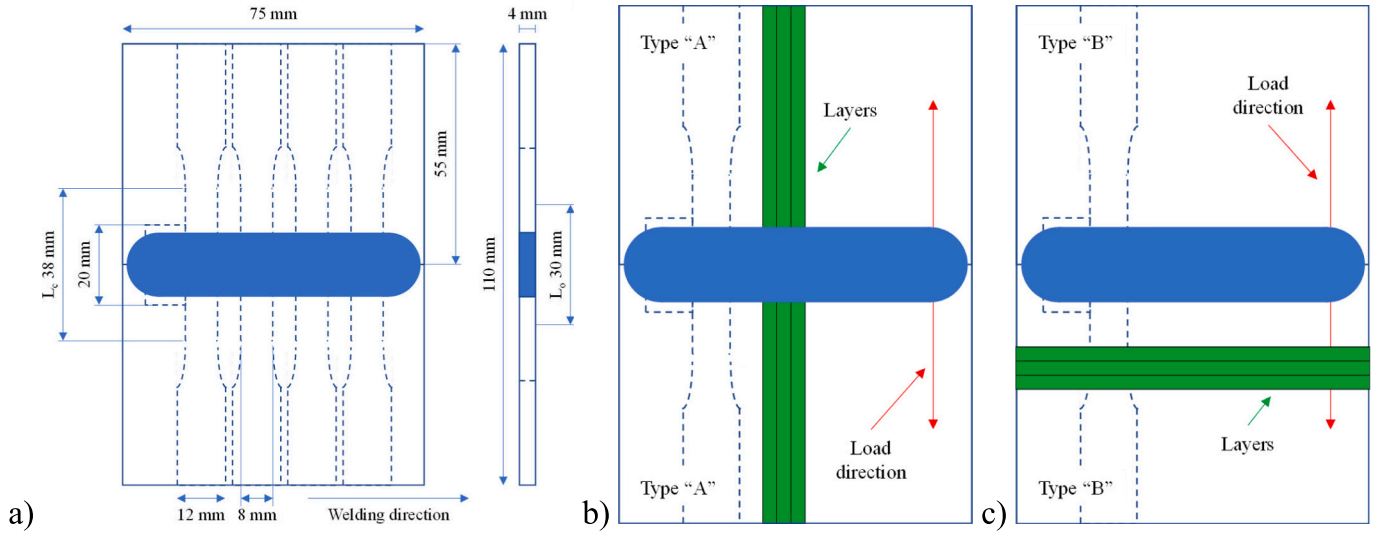

Fig. 3. Sketch of a) the FSW welds, tensile, and metallographic samples. Images b) and c) show the position of the tensile specimens with respect to the build direction of the printed layers.

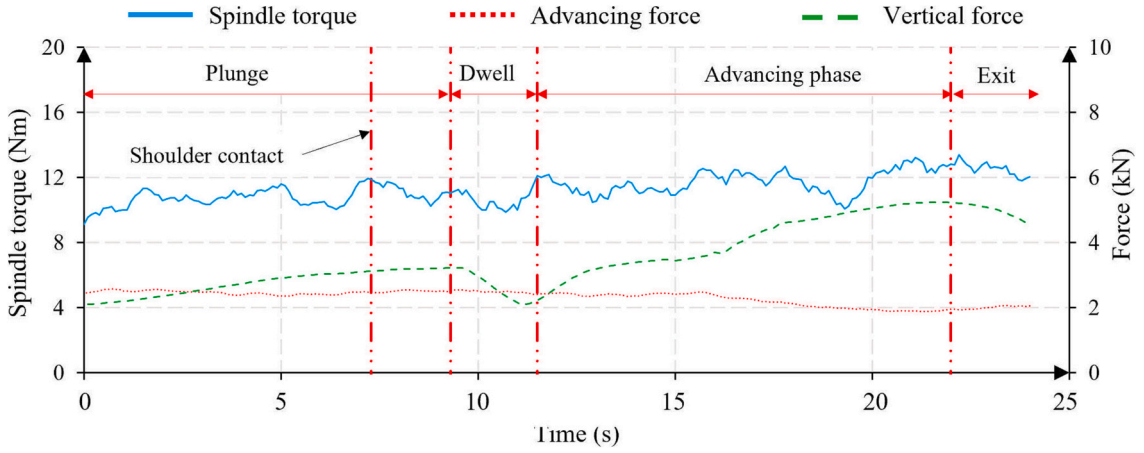

Fig. 4. Monitored spindle torque, advancing and vertical forces during the FSW of Scalmalloy®.

increases to about 2 kN when the pin touches and penetrates the upper plate. The vertical force increases continuously during the tool plunge (i.e., vertical tool penetration in the sheet stack). The force reaches about 3.5 kN after the shoulder touches (about 7 s) and penetrates the upper plate. A metal softening characterized the dwell phase because of the tool friction. As a result, the vertical force reduces to 2 kN. The vertical force increases when the tool starts to move along the welding line because of the resistance of the metal to stirring, reaching a peak value of 5 kN. The vertical force again reduces toward the end of the welding process when the tool/plate friction provides sufficient heat to adequately soften the metal in front of the advancing tool. The advancing force remains constant at 2–3 kN. The spindle torque exhibits an uneven but monotonic increase throughout the welding cycle. Initially, it is 9 Nm, and then progressively increases over 12 Nm in the welding phase.

In FSW, the rotation speed, welding speed, and plunge depth are the most critical process parameters. Their settings strongly influence the thermal input and the metal stirring involved during the joining process, hence the resulting microstructure and mechanical properties of the welded joints. The review of Yang et al. [31] on FSW of aluminum alloys has summarized that rotation speed is the main process parameter affecting weld quality. Higher rotation speeds are beneficial for the mechanical strength of FSW joints because they increase the heat input, thus favoring metal stirring and preventing defects (e.g., lazy S defect, tunneling). However, excessive rotation speeds widen the HAZ and promote grain growth, which negatively influence weld strength. The temperature field and the maximum temperature reached during welding have a more crucial role in heat-treatable aluminum alloys, because they also affect the precipitation and coarsening of the strengthening particles in the matrix and, in turn, the mechanical properties of the joints. Excessive temperatures for prolonged times bring to an overaging of the joint microstructure, limiting joint strength, as also discussed in this work. Contrarily, the heat input reduces with welding speed. This parameter should be selected according to the rotation speed to provide a proper heat input to join aluminum alloys effectively [31]. The influence of the plunge depth on the heat input depends highly on the tool shape. Some tool shapes (e.g., threaded and triflute pins) are more effective for metal stirring and fragmenting the microstructure keeping a low grain size [32]. In this work, the plunge depth has been selected to ensure proper welding of the root of the joint and to limit the formation of flash along the weld seam.

3.2. *Microstructure and hardness examinations*

After metal printing, Scalmalloy® shows the typical lenticular regions caused by the discontinuous melting of the powder layer and its

subsequent solidification, Fig. 5. The geometry and the size of these regions mainly depend on the laser features (e.g., spot, power, scanning speed) and powder layer (e.g., chemical composition, thickness, density, particle size distribution). The bi-modal grain size of the lenticular regions results from the heat transfer that occurs during solidification. Several nucleation sites initially form on the previous layer due to the higher heat transfer and a possible residual of any unmelted powder. Columnar grains then elongate along the maximum direction of the heat transfer because of competitive growth. According to Spierings et al. [33], the marked pinning effect of small Al-Sc phases precipitating along grain boundaries contributes to the fine microstructure. It also hinders grain growth from the heat input released in the subsequent overlapping layers.

The EBSD images in Fig. 6 highlight the grain size of Scalmalloy® in the as-printed condition, Fig. 6 a), and after the aging heat treatment, Fig. 6 b). The fine microstructure of the as-printed Scalmalloy® has an average grain size of 1.5 μm, while the largest columnar grains can be elongated to over 10 μm. Literature shows that Al_3(Sc, Zr) is the most prominent strengthening particle dispersed throughout the metal matrix [34,35]. The grain size distribution of Fig. 7 shows that the grain size of Scalmalloy® only increases slightly because of the aging heat treatment. The average grain size increases from 2.5 to 2.7 μm, while the median value remains almost unchanged. This can be attributed to the marked pinning effect of the Al-Sc precipitates [16,33].

Figs. 8 a) and b) respectively show the typical cross-section of an FSW joint with its characteristic regions and the top view of the welding seam. The build direction does not influence the joint appearance because the stirring action of the tool completely modifies the original microstructures. The metal stirring is asymmetric due to the inhomogeneous material flow on the advancing (AS) and retracting sides (RS). The stronger material flow in AS causes the formation of an evident line that delimitates the SZ from the TMAZ, while it is less detectable on the RS side. The larger extent of the TMAZ region in RS is a consequence of the progressive deceleration of the material flow [21,24]. The cross-section of the FSW joint shows that the tool stirring has eliminated the intrinsic porosity of the as-printed metal in the SZ and limited it in the TMAZ.

Some FSW joints exhibit a lazy S defect (also known as joint line remnant or kissing bond defect) in the center of the SZ. Fig. 8 c) shows a detail of this defect. It has a thickness between 2 and 5 μm and is surrounded by the fine equiaxed microstructure of the SZ. This defect appears in FSW joints due to a redistribution of oxide layers (on the faying surfaces of the two sheets) in the weld nugget [36,37] and has also been found in FSW of heat-treatable aluminum alloys, including 6xxx [38] and 2xxx [39] series. As discussed thereafter, this defect has not had effects on the joint strength and fracture mode of the Scalmalloy® welded samples. Indeed, the welded samples did not fracture along or close the lazy S defects.

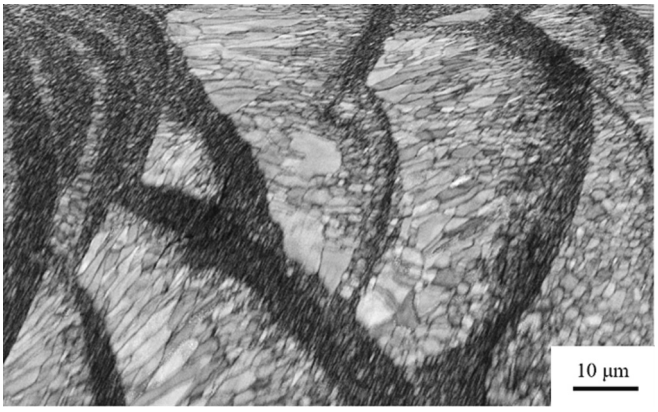

Fig. 5. Lenticular microstructure of the as-printed Scalmalloy®.

Fig. 9 shows the EBSD images captured from the SZ in the as-printed condition, Fig. 9 a), and after the aging heat treatment, Fig. 9 b). The stirring action of the tool completely modified the bi-modal microstructure of Scalmalloy®. The grains were at first highly deformed during the welding and then recrystallized. As a result, the grains in SZ are equiaxed and very fine, with an average grain size of 1.5 μm, Fig. 10 a). Coherently with what occurred for the BM, the aging heat treatment has only had a mild effect on the grain size of the SZ, Fig. 10 b).

The EBSD images of Fig. 11 show the microstructure of the TMAZ of Scalmalloy® joints before and after the aging heat treatment. In this case, the heat treatment has significantly influenced the microstructure of this region. The highly thermo-mechanically deformed grains, Fig. 11 a), have been fully recrystallized by the heat treatment and replaced by new undeformed equiaxed grains close to the SZ. This could be attributed to the greater number of nucleation recrystallization sites along the grain boundaries of the smallest deformed grains. The new microstructure shows some traces of the previous one. The smallest deformed grains close to the SZ have been replaced by many small new grains, while larger new grains far from the SZ are in place of the prior larger deformed grains. Grains far from the SZ show a lower elongation after the heat treatment while still maintaining memory of the previous growth direction.

The EBSD analysis also points out the influence of FSW on the microstructure of the welded joints through the Euler orientation maps. These maps show the crystal orientation of grains through different color patterns. The Euler map of the as-printed Scalmalloy®, Fig. 12 a), shows that the crystals are randomly oriented in the 3d-space regardless the bi-modal microstructure, that is, the LPBF did not introduce a preferential microstructural texture during the layer-by-layer building-up of the plates. This outcome is influenced from the chessboard scanning strategy implemented during the LPBF process. The FSW does not introduce a clear preferential microstructural texture in the SZ because of the recrystallization of this region during the welding process. The fine equiaxed microstructure shows a homogeneous distribution of the color patterns. Preferential crystal orientation is visible in the TMAZ due to the strong metal stirring and a partial or absent grain recrystallization, Fig. 12 b). The Euler map shows that the grains are not only deformed by the metal stirring, but the crystal lattice is also more oriented along the weldment direction (i.e., the blue color is predominant in TMAZ) according to the roto-translation motion of the tool.

The average hardness of the AM as-printed coupon is 120 HV, while the age hardening increased this value to 170 HV. No evident differences have been found between the joints made from the type “A” coupons and those obtained from the type “B” ones because the FSW completely modified the additively manufactured layers. Fig. 13 shows a Vickers microhardness map of the FSW joints before and after age hardening. An asymmetric hardness distribution can be observed due to the different material flows on the AS and the RS. The larger hardness gradient on the AS can be attributed to the stronger material stirring on this joint side. The hardness maps show that the heat input related to the FSW has strongly affected the hardness of the welded joints, Fig. 13 a). The higher heat input developed in the SZ caused by the tool friction has overaged and softened the aluminum matrix. The SZ shows the lowest hardness of 110 HV, which is slightly lower than the as-printed material. As Jiang et al. [41] found, the SZ commonly can reach 500 °C during FSW of aluminum alloys. This temperature is much higher than 350 °C, which has been recognized as promoting the coarsening of Al_3(Sc, Zr) particles [9]. The lower heat input and the strain hardening from metal stirring increase the hardness of TMAZ up to 150 HV, limiting the effect of overaging. In a previous study, Ma et al. [9] demonstrated that the microstructure grain size influences the coarsening of Al_3(Sc, Zr) precipitates: they coarsen to a greater extent when located in a fine equiaxed grain structure (as in the SZ of the FSW joints), while a more limited particle growth occurs in coarse columnar grains (as in the TMAZ). This phenomenon might also have contributed to the considerable hardness gradient between SZ and TMAZ. The heat input has

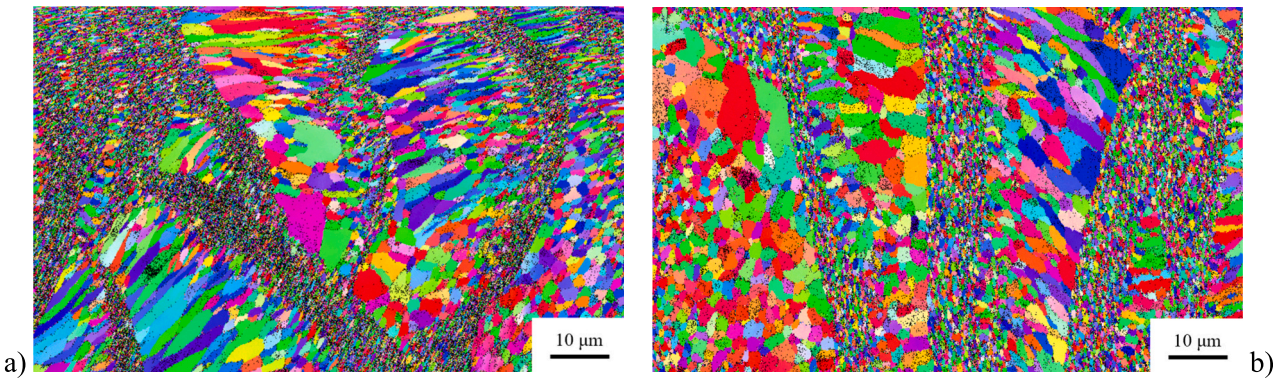

Fig. 6. EBSD images of Scalmalloy® a) before and b) after aging heat treatment.

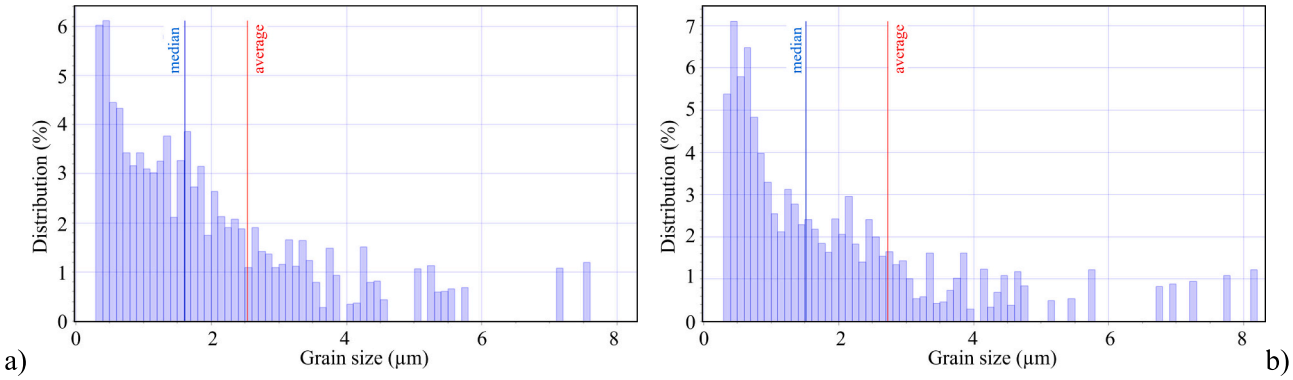

Fig. 7. Grain size distribution (measured according to ASTM E2627 [28]) of Scalmalloy® a) before and b) after the aging heat treatment.

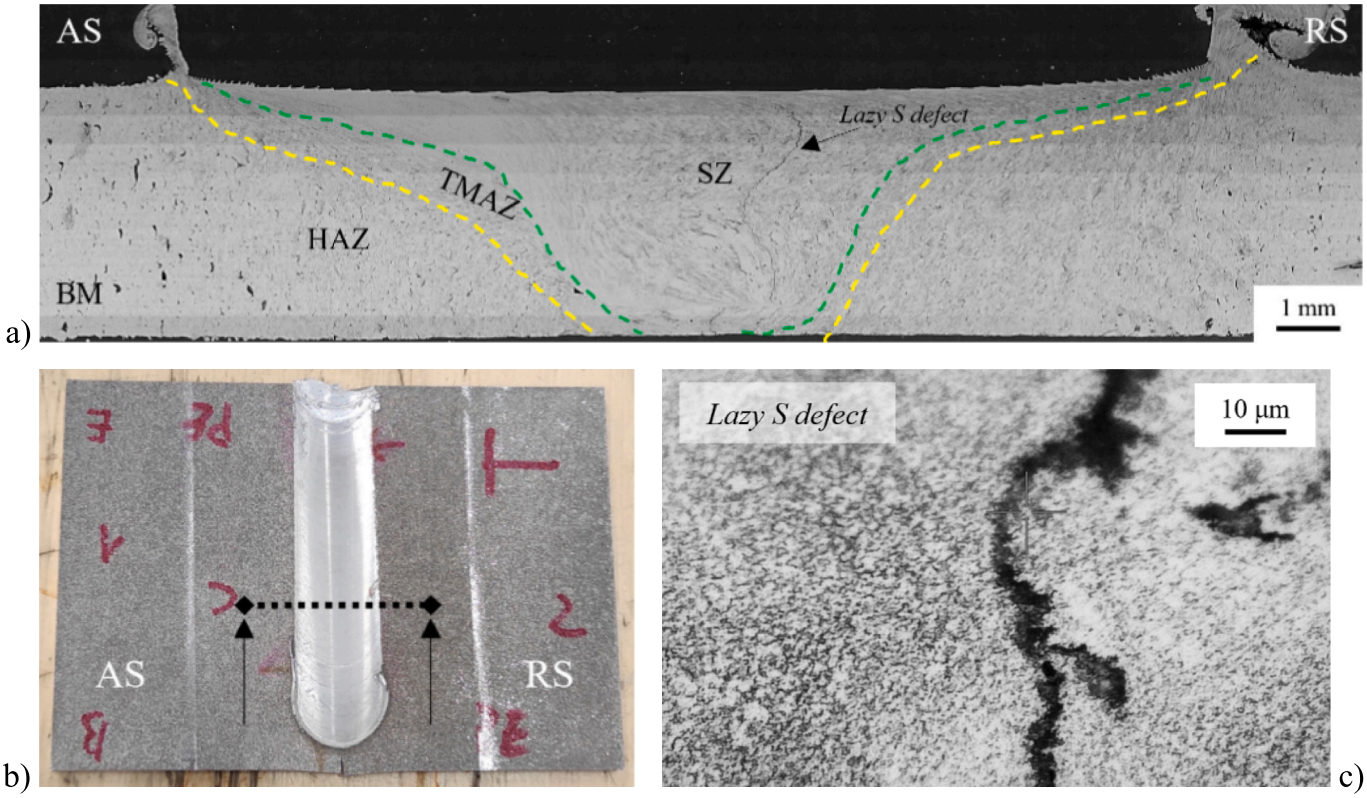

Fig. 8. a) Typical cross-section of an FSW joint, b) top view of the welding seam where the metallographic sample was extracted (black arrows), and c) detail of the lazy S defect.

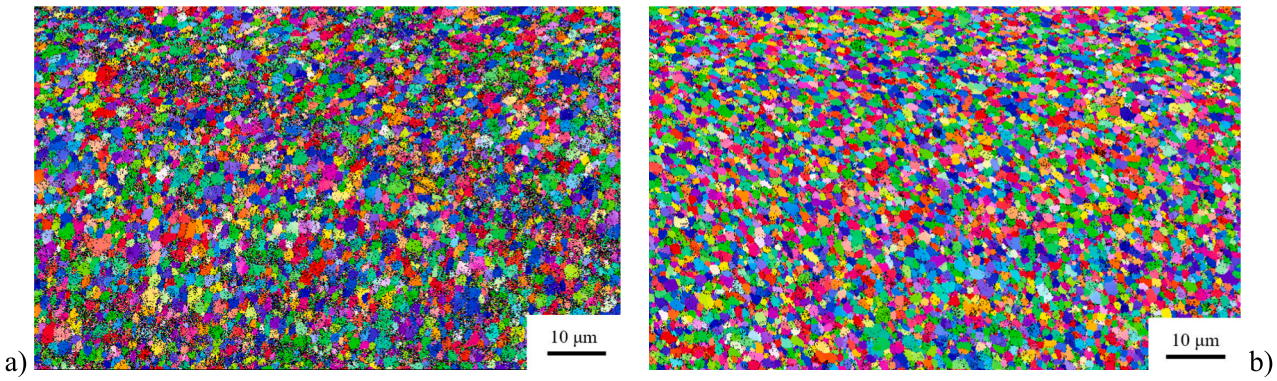

Fig. 9. EBSD images of the SZ of the FSW joints a) before and b) after the aging heat treatment.

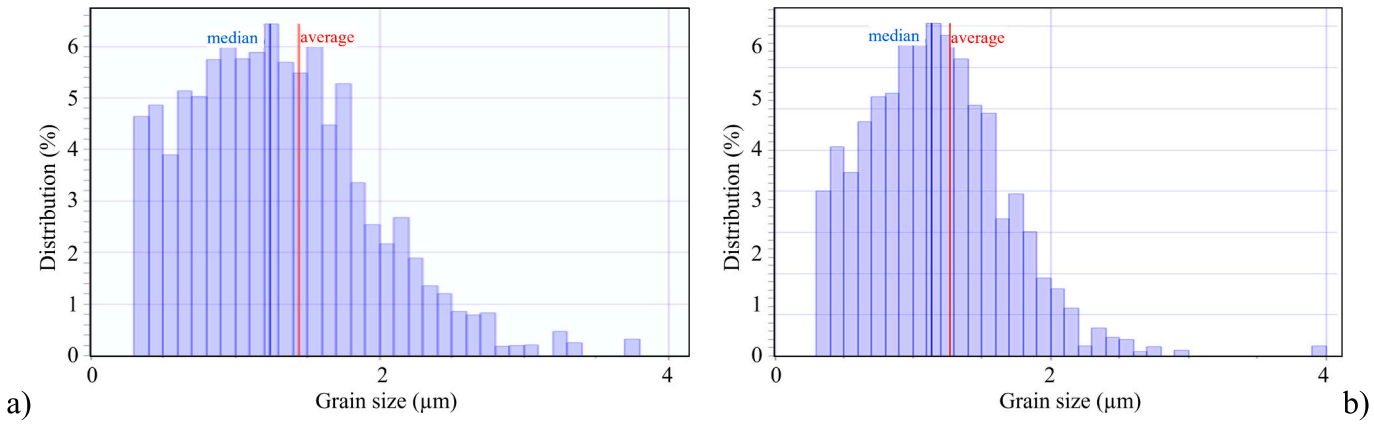

Fig. 10. Grain size distribution (measured according to ASTM E2627 [28]) in the SZ of the FSW welds a) before and b) after the aging heat treatment.

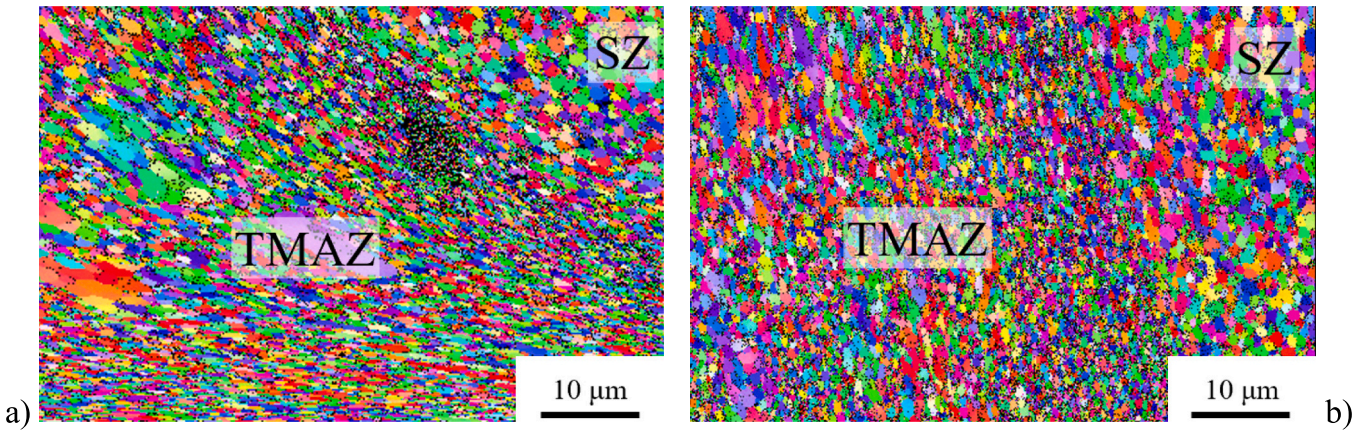

Fig. 11. EBSD images of the TMAZ of the FSW joints a) before and b) after the aging heat treatment.

promoted significant aging in the HAZ. In this region, the hardness increases from 120 to 170 HV. HAZ extends for more than 10 mm from the joint center.

The aging heat treatment has a minimal effect on the hardness of the FSW joints. Comparing Fig. 13 a) and b), hardness slightly increases throughout the welds (about 10 HV). Therefore, aging hardening occurred during welding, while the post-heat treatment has had a mild effect on any further precipitation of Al-Sc particles in the already aged microstructure.

3.3. Joint tensile strength

Fig. 14 shows the results of the tensile test performed on Scalmalloy® under an as-printed condition and after the aging heat treatment. According to the literature [6], Scalmalloy® samples printed with the layers parallel to the tensile direction, type “B”, show a better tensile strength than those with perpendicular layers, type “A”. The better resistance of these samples is related to the orientation of the grains and grain boundaries with respect to the external load. The mechanical strength between grains obtained from two successive layers is always lower than that between grains of the same layer [6]. This also occurs in the Scalmalloy® samples even though the B samples have a lower

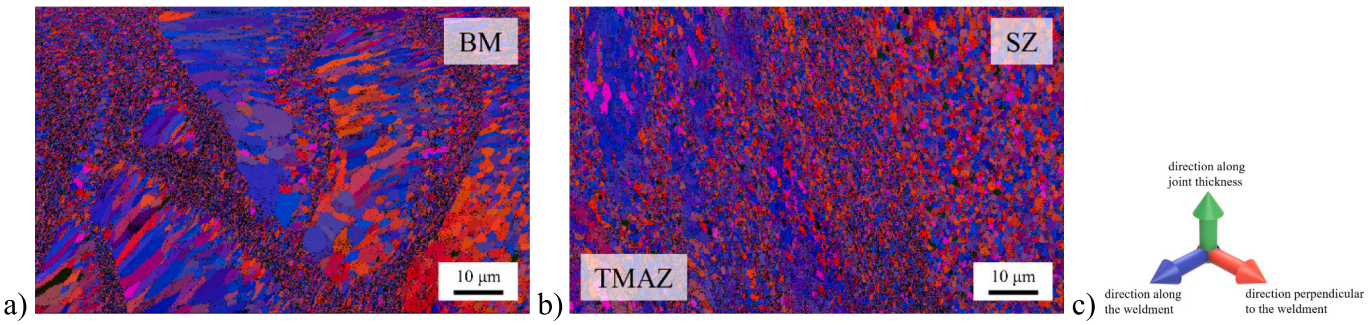

Fig. 12. Euler map of AM Scalmalloy®: a) as-printed condition (BM); b) after FSW and post-heat treatment in the SZ/TMAZ interface at the AS side; c) the colored legend identifies the crystal lattice orientation.

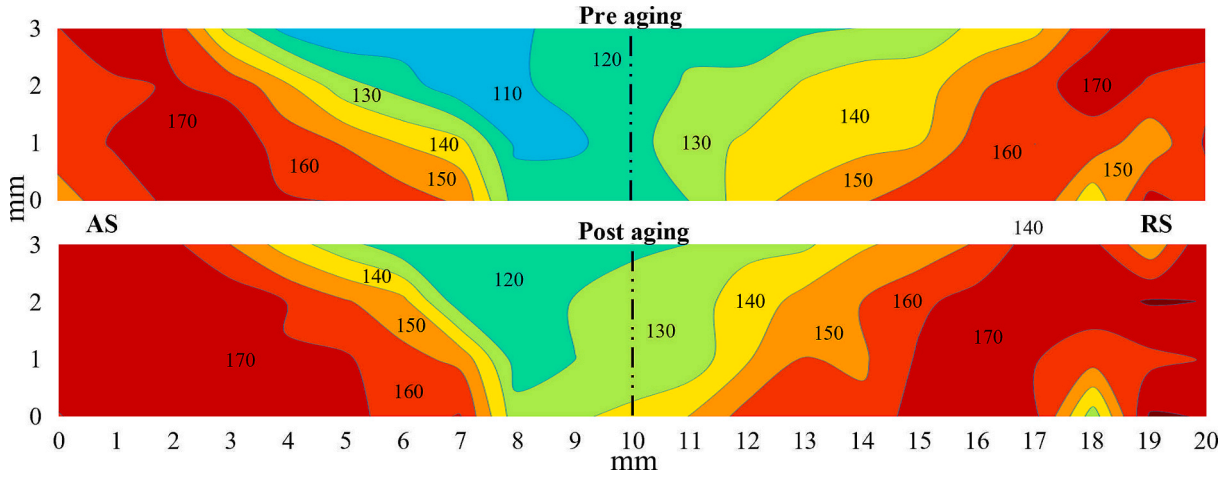

Fig. 13. Vickers microhardness map of an FSW joint before and after the aging heat treatment.

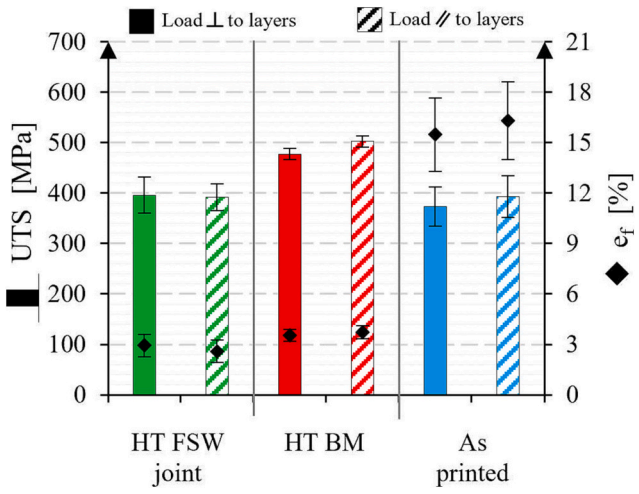

Fig. 14. Results of the tensile tests on as-printed Scalmalloy®, BM, and FSW joints after age hardening: ultimate tensile strength (UTS) and elongation at fracture (e_f). Mean values and standard deviations.

density (98.0 % vs. 99.2 %), hence a large amount of porosity. The average tensile strength of the B samples was 385 MPa, while the elongation at fracture of 17 %. The A samples show slightly lower resistance and ductility, with a strength of 375 MPa and an elongation at fracture of 16 %.

The precipitation of the Al-Sc second phases in the aluminum matrix associated with the age-hardening heat treatment has improved the mechanical strength of Scalmalloy® by about 100 MPa. However, it has a detrimental impact on ductility since the elongation at fracture reduces to 4 % (one-fourth of the value before the heat treatment).

The FSW specimens after the heat treatment show the same strength regardless of the build orientation. This results from the tool stirring action that eliminated any influence of the original layer-by-layer direction. The strength of the heat-treated joints does not vary compared to the as-printed Scalmalloy®. This means that FSW and the following heat treatment have not had a detrimental effect, at least maintaining the same strength as the base material or slightly superior.

The fracture surfaces of the heat-treated samples do not show differences from each other at varying build directions. As shown in Fig. 15 a), the fracture surface of Scalmalloy® exhibits a macroscopic fracture without an appreciable necking. On a microscopic scale, the fracture surface shows mixed brittle-ductile features, Fig. 15 b). Nearly flat facets, commonly associated with a brittle fracture mode, have some ductile features like local extensive plastic deformations. In contrast, dimples appear when examined under higher magnifications, inset of Fig. 15 b). As typically occurs in 3d printed metals, small voids and some regions with unmelted powders have been found because of the incomplete densification of Scalmalloy®.

Regardless of the build direction, all the FSW joints failed similarly, Fig. 16. The fracture surface nucleates at the interface between the TMAZ and the SZ regions, Fig. 15 a). It then propagates through the joint until the necking of the sample and its final fractures. At the end of the failure process, the crack propagated through the SZ on the upper side of the joints and the SZ/TMAZ interface on the lower side. The cross-section of the fracture surface displays the typical cope and cone appearance accompanied by a large amount of plastic deformation. Shear lips are observed at the latter part of the fracture and indicate the

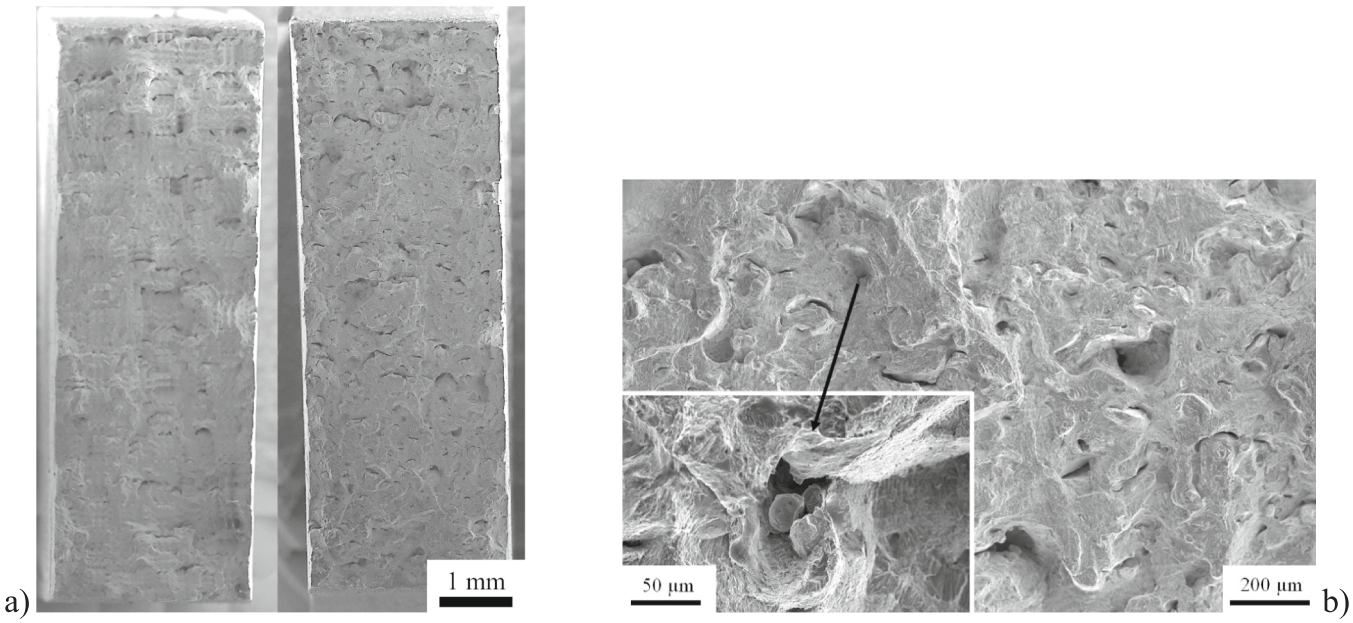

Fig. 15. SEM image of the fracture surface obtained from a) the heat-treated Scalmalloy® ("A" plate) and b) its magnification.

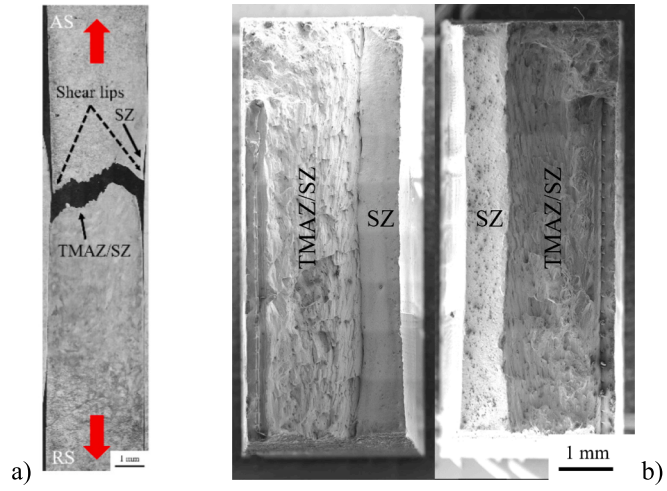

Fig. 16. Macroscopic view of the fractured FSW joints after heat treatment: a) welded tensile samples (the red arrows identify the tensile load during the test) and b) fracture surfaces. (For interpretation of the references to color in this figure legend, the reader is referred to the web version of this article.)

final failure of the welded samples, Fig. 16 a). The FSW joints always have a smaller resistant cross-section area than the rest of the coupons due to the tool plunging. This aspect could have contributed to the formation of the fracture in this location. Moreover, the deformation is localized in this area because it also exhibits the lowest hardness in the joint, see Fig. 13. On a microscopic scale, microvoid coalescence drives the fracture in the SZ, Fig. 17 a). The failure at the SZ/TMAZ interface shows an oriented fracture surface, Fig. 17 b), associated with the strong directional material flow in this region during the tool stirring, see Fig. 12 b). The fracture of the welded samples never occurred through the lazy S defects, if present, making them irrelevant to the mechanical strength of the FSW joints.

4. Conclusions

This work investigates FSW of 4 mm thick Scalmalloy® plates additively manufactured via LPBF to assess the feasibility and the influence of a solid-state technology on the joint strength and quality. The main results are summarized as follows:

- The build direction slightly influences the mechanical strength of the as-printed Scalmalloy®, with the layer parallel to the tensile load that is more resistant even though it has a lower density (98.0 % vs. 99.2 %).

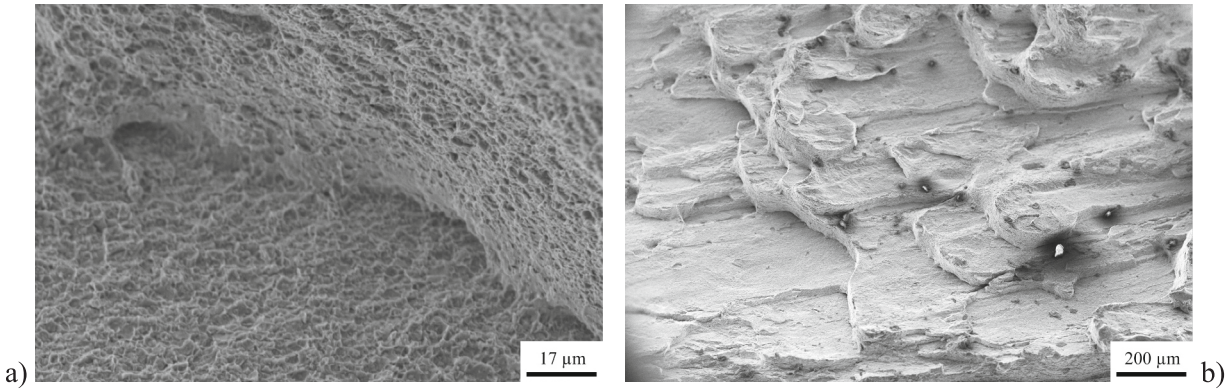

Fig. 17. High magnification of the fracture surface extracted from the a) SZ and b) the interface between the SZ and TMAZ (the locations of these regions are highlighted by the black arrows in Fig. 16 a).

- FSW completely modifies the original microstructures of Scalmalloy®. Metal stirring recrystallizes and refines the grain microstructure of the joints and has a beneficial effect on closing the porosity of the as-printed plates.

- The Al-Sc precipitates have a powerful effect on pinning the grain boundaries. After the aging heat treatment, the grain size remained almost unchanged in the SZ, while the deformed grain in the TMAZ recrystallized, even maintaining a small size.

- The aging heat treatment increases the mechanical strength of Scalmalloy® plates from about 400 to 500 MPa, albeit at the expense of ductility (i.e., elongation at fracture reduces from about 16 % to 4 %. The post-heat treatment slightly improved the tensile strength of the FSW welds (10–20 MPa).

- The FSW joints failed at the SZ/TMAZ interface at the AS where the joints exhibited the lowest hardness.

Overall, FSW can be considered a promising technique to join Scalmalloy® even though some improvements could be obtained by optimizing the heat input and reducing the indentation of the tool shoulder in the upper sheet. In that way, a post-weld aging heat treatment might be unnecessary.

Declaration of competing interest

The authors declare that they have no known competing financial interests or personal relationships that could have appeared to influence the work reported in this paper.

Acknowledgments

This study was supported by “Fondo per la Crescita Sostenibile - D.M. 2/3/2018 – D.D. 26/9/2019 - Bando Accordi di innovazione per la SPACE ECONOMY” - Project number F/230003/01-05/X48; J-Tech@-PoliTO, advanced joining technologies research center at Politecnico di Torino (http://www.j-tech.polito.it/); and by the Pro-M facility (https://promfacility.eu).

References

[1] Czerwinski F. Thermal stability of aluminum alloys. Materials (Basel) 2020;13:3441. https://doi.org/10.3390/ma13153441.
[2] Walachowicz F, Bernsdorf I, Papenfuss U, Zeller C, Graichen A, Navrotsky V, Rajvanshi N, Kiener C. Comparative energy, resource and recycling lifecycle analysis of the industrial repair process of gas turbine burners using conventional machining and additive manufacturing. J Ind Ecol 2017;21:S203–15. https://doi.org/10.1111/jiec.12637.
[3] Davis W, Lunetto V, Priarone PC, Centea D, Settineri L. An appraisal on the sustainability payback of additively manufactured molds with conformal cooling. In: Procedia CIRP; 2020. p. 516–21. https://doi.org/10.1016/j.procir.2020.01.064.
[4] Kolobnev NI. Aluminum-lithium alloys with scandium. Met. Sci. Heat Treat. 2002;44:297–9. https://doi.org/10.1023/A:1021207921163.
[5] Rometsch PA, Zhu Y, Wu X, Huang A. Review of high-strength aluminium alloys for additive manufacturing by laser powder bed fusion. Mater Des 2022;219:110779. https://doi.org/10.1016/j.matdes.2022.110779.
[6] Spierings AB, Dawson K, Voegtlin M, Palm F, Uggowitzer PJ. Microstructure and mechanical properties of as-processed scandium-modified aluminium using selective laser melting. CIRP Ann 2016;65:213–6. https://doi.org/10.1016/j.cirp.2016.04.057.
[7] Martucci A, Aversa A, Manfredi D, Bondioli F, Biamino S, Ugues D, Lombardi M, Fino P. Low-power laser powder bed fusion processing of Scalmalloy®. Materials (Basel) 2022;15:3123. https://doi.org/10.3390/ma15093123.
[8] Qbau N, Nam ND, Ca NX, Hien NT. The crack healing effect of scandium in aluminum alloys during laser additive manufacturing. J Manuf Process 2020;50:241–6. https://doi.org/10.1016/j.jmapro.2019.12.050.
[9] Ma R, Peng C, Cai Z, Wang R, Zhou Z, Li X, Cao X. Manipulating the microstructure and tensile properties of selective laser melted Al–Mg-sc-zr alloy through heat treatment. J Alloys Compd 2020;831:154773. https://doi.org/10.1016/j.jallcom.2020.154773.
[10] Schmidtke K, Palm F, Hawkins A, Emmelmann C. Process and mechanical properties: applicability of a scandium modified Al-alloy for laser additive manufacturing. Phys Procedia 2011;12:369–74. https://doi.org/10.1016/j.phpro.2011.03.047.
[11] Zhang H, Gu D, Yang J, Dai D, Zhao T, Hong C, Gasser A, Poprawe R. Selective laser melting of rare earth element sc modified aluminum alloy: thermodynamics of precipitation behavior and its influence on mechanical properties. Addit Manuf 2018;23:1–12. https://doi.org/10.1016/j.addma.2018.07.002.
[12] Spierings AB, Dawson K, Kern K, Palm F, Wegener K. SLM-processed sc- and zr-modified Al-mg alloy: mechanical properties and microstructural effects of heat treatment. Mater Sci Eng A 2017;701:264–73. https://doi.org/10.1016/j.msea.2017.06.089.
[13] Xiao X, Qin D, Mao Y, Fu L. Effects of pin morphology on the interface defects of the FSWed lap joints of 2A12 aluminum alloy. J Manuf Process 2021;68:128–40. https://doi.org/10.1016/j.jmapro.2021.05.023.
[14] Kashaev N, Ventzke V, Çam G. Prospects of laser beam welding and friction stir welding processes for aluminum airframe structural applications. J Manuf Process 2018;36:571–600. https://doi.org/10.1016/j.jmapro.2018.10.005.
[15] Zhao J, Jiang F, Jian H, Wen K, Jiang L, Chen X. Comparative investigation of tungsten inert gas and friction stir welding characteristics of Al–Mg–Sc alloy plates. Mater Des 2010;31:306–11. https://doi.org/10.1016/j.matdes.2009.06.012.
[16] Sauvage X, Dédé A, Muñoz AC, Huneau B. Precipitate stability and recrystallisation in the weld nuggets of friction stir welded Al–Mg–Si and Al–Mg–Sc alloys. Mater Sci Eng A 2008;491:364–71. https://doi.org/10.1016/j.msea.2008.02.006.
[17] Malopheyev S, Mironov S, Kulitskiy V, Kaibyshev R. Friction-stir welding of ultra-fine grained sheets of Al–Mg–Sc–Zr alloy. Mater Sci Eng A 2015;624:132–9. https://doi.org/10.1016/j.msea.2014.11.079.
[18] TWI LIMITED. Optimisation of friction stir welding (FSW) and laser beam welding (LBW) for assembly of structural aircraft parts. 2020. https://doi.org/10.3030/785557.
[19] Scherillo F, Astarita A, Prisco U, Contaldi V, di Petta P, Langella A, Squillace A. Friction stir welding of AlSi10Mg plates produced by selective laser melting. Metallogr Microstruct Anal 2018;7:457–63. https://doi.org/10.1007/s13632-018-0465-y.
[20] Du Z, Tan MJ, Chen H, Bi G, Chua CK. Joining of 3D-printed AlSi10Mg by friction stir welding. Weld World 2018;62:675–82. https://doi.org/10.1007/s40194-018-0585-7.
[21] Moeini G, Sajadifar SV, Wegener T, Rössler C, Gerber A, Böhm S, Niendorf T. On the influence of build orientation on properties of friction stir welded Al–Si10Mg parts produced by selective laser melting. J Mater Res Technol 2021;12:1446–60. https://doi.org/10.1016/j.jmrt.2021.03.101.
[22] Eff M, Hack H, Shipley D, Shira S. The effects of postweld processing on friction stir welded, additive manufactured AlSi10Mg. Weld J 2022;101:111–22. https://doi.org/10.29391/2022.101.009.
[23] Prashanth KG, Damodaram R, Scudino S, Wang Z, Prasad Rao K, Eckert J. Friction welding of Al–12Si parts produced by selective laser melting. Mater Des 2014;57:632–7. https://doi.org/10.1016/j.matdes.2014.01.026.
[24] Moeini G, Sajadifar SV, Wegener T, Brenne F, Niendorf T, Böhm S. On the low-cycle fatigue behavior of friction stir welded Al–Si12 parts produced by selective laser melting. Mater Sci Eng A 2019;764:138189. https://doi.org/10.1016/j.msea.2019.138189.
[25] Li R, Chen H, Zhu H, Wang M, Chen C, Yuan T. Effect of aging treatment on the microstructure and mechanical properties of Al-3 . 02Mg-0 . 2Sc-0 . 1Zr alloy printed by selective laser melting. Mater. Des. 2019;168:107668. https://doi.org/10.1016/j.matdes.2019.107668.
[26] Jia Q, Zhang F, Rometsch P, Li J, Mata J, Weyland M, Bourgeois L, Sui M, Wu X. Precipitation kinetics, microstructure evolution and mechanical behavior of a developed Al À Mn À Sc alloy fabricated by selective laser melting. Acta Mater 2020;193:239–51. https://doi.org/10.1016/j.actamat.2020.04.015.
[27] Deutsches Institut für Normung. In: DIN 50125:2016-12. Testing of metallic materials - Tensile test pieces; 2016. p. 17. https://www.beuth.de/de/norm/din-50125/262241217.
[28] ASTM. In: ASTM E2627. Standard practice for determining average grain size using electron backscatter diffraction (EBSD) in fully recrystallized polycrystalline materials; 2019. p. 5. https://doi.org/10.1520/E2627-13R19.
[29] Adam DPF, Schwartz J, Kumar Mukul, Adams Brent L. Electron backscatter diffraction in materials science. Boston, MA: Springer, US; 2009. https://doi.org/10.1007/978-0-387-88136-2.
[30] ASTM International. Standard test methods for vickers hardness and knoop hardness of metallic materials ASTM E92. 2017. https://doi.org/10.1520/E0092-17.
[31] Yang Y, Bi J, Liu H, Li Y, Li M, Ao S, Luo Z. Research progress on the microstructure and mechanical properties of friction stir welded Al Li alloy joints. J. Manuf. Process. 2022;82:230–44. https://doi.org/10.1016/j.jmapro.2022.07.067.
[32] Banik A, Barma JDeb, Saha SC. Effect of threaded pin tool for friction stir welding of AA6061-T6 at varying traverse speeds: torque and force analysis. Iran. J. Sci. Technol. Trans. Mech. Eng. 2020;44:749–64. https://doi.org/10.1007/s40997-019-00289-w.
[33] Spierings AB, Dawson K, Heeling T, Uggowitzer PJ, Schäublin R, Palm F, Wegener K. Microstructural features of Sc- and Zr-modified Al-mg alloys processed by selective laser melting. Mater Des 2017;115:52–63. https://doi.org/10.1016/j.matdes.2016.11.040.
[34] Fuller C, Seidman D. Temporal evolution of the nanostructure of Al(Sc, Zr) alloys: part II-coarsening of Al(ScZr) precipitates. Acta Mater 2005;53:5415–28. https://doi.org/10.1016/j.actamat.2005.08.015.
[35] Kendig KL, Miracle DB. Strengthening mechanisms of an Al-mg-sc-zr alloy. Acta Mater 2002;50:4165–75. https://doi.org/10.1016/S1359-6454(02)00258-6.
[36] Safeen MW, Russo Spena P. Main issues in quality of friction stir welding joints of aluminum alloy and steel sheets. Metals (Basel) 2019;9:610. https://doi.org/10.3390/met9050610.

[37] Mishra RS, Mahoney MW, editors. Friction Stir Welding and Processing. ASM International; 2007. ISBN: 978-0-87170-840-3.
[38] Mahto RP, Gupta C, Kinjawadekar M, Meena A, Pal SK. Weldability of AA6061-T6 and AISI 304 by underwater friction stir welding. J Manuf Process 2019;38:370–86. https://doi.org/10.1016/j.jmapro.2019.01.028.
[39] Masoumi Khalilabad M, Zedan Y, Texier D, Jahazi M, Bocher P. Effect of tool geometry and welding speed on mechanical properties of dissimilar AA2198–AA2024 FSWed joint. J Manuf Process 2018;34:86–95. https://doi.org/10.1016/j.jmapro.2018.05.030.